Phase separation in the CoO_2 layer observed in thermoelectric layered cobalt dioxides

Tsuyoshi Takami,[1,*] Hiroshi Nanba,[1] Yasuhide Umeshima,[1] Masayuki Itoh,[1] Hiroshi Nozaki,[2] Hiroshi Itahara,[2] and Jun Sugiyama[2]

[1]*Department of Physics, Graduate School of Science, Nagoya University, Furo-cho, Chikusa-ku, Nagoya 464-8602, Japan*

[2]*Toyota Central Research and Development Laboratories, Inc., Nagakute, Aichi 480-1192, Japan*

(Received 5 June 2009; revised manuscript received 12 October 2009; published 4 January 2010)

^{59}Co nuclear magnetic resonance (NMR) measurements have been performed to study the local magnetic properties of the misfit layered cobalt dioxides (MLCO's) with the CoO_2 and rock-salt layers, $[Ca_2CoO_3]_{0.62}CoO_2$ ($\equiv Ca_3Co_{3.92}O_{9.34}$) and $Ca_3Co_{3.92}O_{9.34-\delta}$ with oxygen nonstoichiometry. The ^{59}Co NMR spectrum consists of mainly five lines at 4.2 K at which the samples are in a magnetically ordered state. Among the five NMR lines for $Ca_3Co_{3.92}O_{9.34}$, three lines at higher frequencies (f's) satisfy the resonance condition with two branches indicating the presence of antiferromagnetic internal fields (H_{int}'s). The other two lines exhibit one branch, and one of the two has a nonzero H_{int} under zero external field (ZF), which signifies the existence of ferromagnetic (FM) H_{int}'s. The other has a zero H_{int} under ZF. By taking account of both the valence state of the Co ions in each layer and the lattice modulation due to the misfit between the CoO_2 layer and the rock-salt layer, the NMR spectra at higher f's are attributed to the Co in the rock-salt layer, whereas those at lower f's to the Co in the CoO_2 layer. Furthermore, a spin-density wave order appears to coexist with a FM order in the CoO_2 layer for MLCO's. The magnetic and transport properties of these materials are discussed in terms of a separation between two phases.

DOI: 10.1103/PhysRevB.81.014401 PACS number(s): 72.15.Jf, 75.50.Gg, 75.30.Fv

I. INTRODUCTION

Since the discovery[1] of the coexistence of a large thermopower and a low electrical resistivity in $NaCo_2O_4$, which has a close-packed two-dimensional (2D) CoO_2 array, extensive investigations of other cobalt oxides have been undertaken in a search for practical materials for thermoelectric conversion. Furthermore, the sodium content x in Na_xCoO_2 can be varied over a wide range, and this system has been reported to show various magnetic and electrical properties with changing x and/or T, such as superconductivity for water intercalated $Na_{0.35}CoO_2$,[2] a charge ordered state for $Na_{0.5}CoO_2$,[3] and a spin-density wave (SDW) ordered state for Na_xCoO_2 with $x \geq 0.75$.[4] These experimental findings have also drawn much interest in the inter-relationship between dimensionality and physical/transport properties among the cobalt oxides.

For instance, perovskite-type $R_{1-x}Sr_xCoO_3$ (R=La, Pr, Nd, and Sm) with x=0.05–0.1 could be potential thermoelectric materials at around room temperature.[5–7] Their structure consists of corner-sharing CoO_6 octahedra forming a three-dimensional (3D) network. However, none of the Co-oxide perovskites can be used at high T because their thermopower decreases rapidly above $\approx$500 K due to a spin-state transition and/or a metal-insulator transition.

In contrast to the 3D system, the quasi-one-dimensional (Q1D) cobalt oxides, $A_{n+2}Co_{n+1}O_{3n+3}$ (A: alkaline-earth metal, n=1–5 and ∞), in which each 1D CoO_3 chain is surrounded by six equally spaced chains forming a triangular lattice in the ab plane, exhibit no spin-state transition at least between 2–600 K.[8–10] The unusual magnetic properties, such as a partially disordered antiferromagnetic state, were found in $Ca_3Co_2O_6$ (A=Ca, n=1),[11,12] which is a 2D antiferromagnet with ferromagnetic (FM) Ising-spin chains, and the magnetic phase diagram with various n has been proposed from positive muon spin rotation and relaxation (μ^+SR) and magnetization measurements.[8–10,13] Partially due to the lack of a spin-state transition and their chemical stability, at least up to 1300 K, the Q1D cobalt oxides with n=1 and 2 have been suggested to be potential candidates for thermoelectric materials at $\approx$1300 K.[14,15]

For the Q1D and 3D systems, the dimensionless figure of merit $ZT=S^2T/\rho\kappa$, which is related to the efficiency and performance of thermoelectric power generation or cooling, is still not high enough for practical application; further investigations to improve their thermoelectric properties are needed as far as we know. Here, S, ρ, κ, and T are thermopower, electrical resistivity, thermal conductivity, and absolute temperature, respectively. On the other hand, misfit layered cobalt dioxides (MLCO's), $[Ca_2CoO_3]_{0.62}CoO_2$ and $[Ca_2Co_{1.3}Cu_{0.7}O_4]_{0.62}CoO_2$, have attracted considerable attention because of their large S, low ρ, and low κ, as in the case of Na_xCoO_2. In particular, MLCO's exhibit excellent thermoelectric performance at high T compared to Na_xCoO_2,[16,17] since MLCO's are more stable at high T than Na_xCoO_2. Structurally, MLCO's share common components, CoO_2 and rock-salt layers. The CoO_2 layer consists of a 2D triangular lattice of edge-sharing CoO_6 octahedra in the ab plane. In the rock-salt layer, on the other hand, cations and the O^{2-} ions make a rock-salt lattice. Triple and quadruple subsystems form the rock-salt layer in $[Ca_2CoO_3]_{0.62}CoO_2$ and $[Ca_2Co_{1.3}Cu_{0.7}O_4]_{0.62}CoO_2$, respectively. The overall crystal structure of these materials consists of alternating layers of the CoO_2 and rock-salt layers stacked along the c axis. In addition, there is a misfit between the two layers along the b axis, i.e., the spatial period along the b axis of the CoO_2 layer is incommensurate with that of the rock-salt layer.

Motivated by the geometrical frustration in the CoO_2 layer for $[Ca_2CoO_3]_{0.62}CoO_2$ and $[Ca_2Co_{1.3}Cu_{0.7}O_4]_{0.62}CoO_2$ with 2D triangular lattices, the magnetic nature of these compounds has also been actively studied. μ^+SR and magnetiza-

 ©2010 The American Physical Society

tion experiments on $[Ca_2CoO_3]_{0.62}CoO_2$ indicated the existence of a short-range order of an incommensurate (IC) SDW state below $\approx$100 K; a long-range IC-SDW order was completed below $\approx$30 K.[18,19] ρ increases drastically upon cooling particularly below 100 K.[16] With a further decrease in T, the ferrimagnetic (FR) transition was reported to take place at $\approx$19 K.[18,19] Also, $[Ca_2Co_{1.3}Cu_{0.7}O_4]_{0.62}CoO_2$ exhibits similar magnetic transitions, i.e., a SDW state and a magnetically ordered state, but the onset of the transition T's to the ordered states are higher than those for $[Ca_2CoO_3]_{0.62}CoO_2$. That is, a transition to a short-range order of the IC-SDW state at $\approx$180 K with decreasing T was found; then the long-range order and a 3D antiferromagnetic (AF) (or FR) order appeared below $\approx$140 and $\approx$85 K, respectively.[20] Quite recently, we have performed ^{59}Co nuclear magnetic resonance (NMR) measurements on the latter compound, and the observed ^{59}Co NMR spectra with varying T were in agreement with the phase diagram.[21]

In the lattice of MLCO's, there are at least two Co sites, namely, one is in the CoO_2 layer and the other is in the rock-salt layer. This is partially, to our knowledge, the predominant reason for the complex magnetic properties of the MLCO's. In particular, the charge-carrier transport of the MLCO's is restricted mainly to the CoO_2 layer, which means that the transport properties are mostly governed by electrons in this layer. Interestingly, the degeneracy of spins and orbitals of the 3d electrons of the Co ions has been theoretically pointed out to be important for enhancing S.[22] However, the local magnetic properties in each layer of MLCO's have not been fully established in contrast to Na_xCoO_2. This situation is partially due to the complex crystal structure and the difficulty in controlling widely the carrier density in the CoO_2 layer by changing the amount of cations. Recently, it has been reported that the transport properties of an MLCO also depend on their oxygen deficiency (δ),[23] as well as on x for Na_xCoO_2. Therefore, a systematic study with changing δ and the number of the rock-salt layers could be one way to address this issue.

In this paper, in order to clarify the local magnetism in each layer and understand the mechanism of the excellent thermoelectric properties of the MLCO's, we have performed ^{59}Co NMR measurements on $[Ca_2CoO_3]_{0.62}CoO_2$ ($\equiv Ca_3Co_{3.92}O_{9.34}$) and $Ca_3Co_{3.92}O_{9.34-\delta}$ with δ=0.34, together with a c-axis-aligned sample of $Ca_3Co_{3.92}O_{9.34-\delta}$ with δ=0.24. We report the NMR results on the three samples with different oxygen contents in detail and compare the results with those on the other MLCO, $[Ca_2Co_{1.3}Cu_{0.7}O_4]_{0.62}CoO_2$.

II. EXPERIMENT

The polycrystalline samples of $Ca_3Co_{3.92}O_{9.34}$ and $Ca_3Co_{3.92}O_{9.34-\delta}$ used in this study were prepared by solid-state reaction. A mixture of the starting materials, $CaCO_3$ and Co_3O_4 powders, was pressed into pellets and calcined at 900 °C for 20 h in an O_2 flow. After regrinding, the powders were pelletized and calcined again under the same conditions. This process was repeated several times in order to obtain well-crystallized single-phase samples. The deoxygenation was carried out in pure N_2 gas with high purity (99.9998%) according to Ref. 23. The c-axis-aligned $Ca_3Co_{3.92}O_{9.34-\delta}$ sample was synthesized by a reactive templated grain growth technique at Toyota Central Research and Development Laboratories. Inc.[24] Diffraction peaks only from (00l) planes were observed for this sample. The Lotgering factor was estimated to be over 0.95 using the x-ray diffraction intensity, indicative of a strong c-axis orientation. Further detailed preparation and characterization of this sample have been already published elsewhere.[25] The oxygen contents in the deoxygenated sample and the c-axis-aligned sample were chemically determined by iodometric titration and were found to be 9 and 9.1, respectively.

X-ray diffraction measurements were carried out with Cu $K\alpha$ radiation to confirm the phase purity. All the x-ray diffraction peaks of the MLCO's studied in this work were indexed by a monoclinic unit cell consistent with the literature,[17,26] indicating that these samples are single phase. The c-axis length increased with δ, while the change in the a-axis length was quite small. The two b-axis lengths exhibited an opposite trend with increasing δ, i.e., the $b1$-axis length for the CoO_2 layer increased, whereas the $b2$-axis length for the rock-salt layer decreased. These results are consistent with the previous study.[23] We have further tested the phase purity by NMR measurements, which are more sensitive compared to x-ray diffraction measurements. Impurity phases, such as Co_3O_4 and $Ca_3Co_2O_6$, were not observed in the NMR spectrum. These results suggest that we successfully obtained MLCO's of high purity. NMR measurements were performed using a coherent pulsed spectrometer and a superconducting magnet with a constant field of H =6.1065 T. ^{59}Co NMR spectra in the field were obtained after Fourier transformation of spin-echo signals collected at some frequencies (f's). F-swept NMR spectra under zero external field (ZF) were also taken point by point of f.

III. RESULTS

A. Randomly oriented polycrystalline $Ca_3Co_{3.92}O_{9.34}$

In a magnetically ordered state, in general, the nuclei are subjected to an internal field (H_{int}) due to the spontaneous magnetic moments. Consequently, an NMR spectrum can be detected even under ZF. The f-swept ^{59}Co NMR spectrum at 4.2 K under ZF was measured in the wide f range up to 300 MHz, which is shown in Fig. 1(a). Following the general trend, we observed a ^{59}Co NMR spectrum with several components in the FR state under ZF. This result clearly demonstrates the existence of nonequivalent Co sites with different H_{int}'s. Note here that the NMR lines corresponding to small H_{int}'s are distributed near 0 MHz in the ZF-NMR spectrum. Therefore, although it is difficult to detect these NMR lines in this measurement condition, the presence of the two components, S1 and S2, is confirmed by other measurement conditions in later, i.e., the T dependence of the NMR spectrum under an external field H and the H dependence of the resonance f as discussed below. By taking account of both the valence state of Co in each layer and the lattice modulation due to the misfit,[16,26] we have concluded that the NMR spectra for S3–S5 are attributed to the Co in the rock-salt layer,

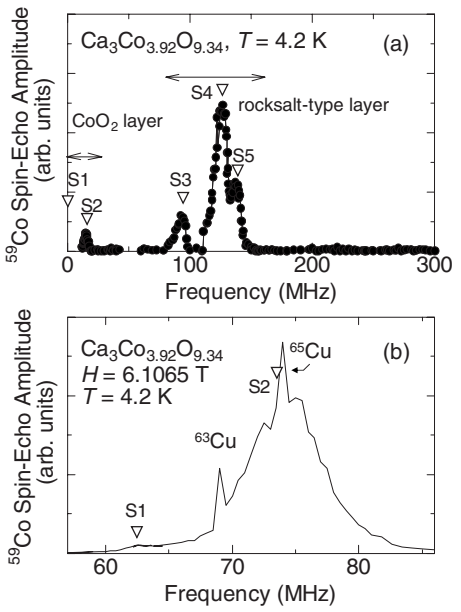

FIG. 1. Frequency-swept ^{59}Co NMR spectra for $Ca_3Co_{3.92}O_{9.34}$ at 4.2 K under (a) ZF (Ref. 21) and (b) 6.1065 T. S1–S5 represent the peak positions of the NMR spectra. The solid line in Fig. 1(a) is a guide to the eyes. The peaks observed at 68.91 and 73.82 MHz in Fig. 1(b) are the ^{63}Cu and ^{65}Cu NMR signals in an NMR coil, respectively.

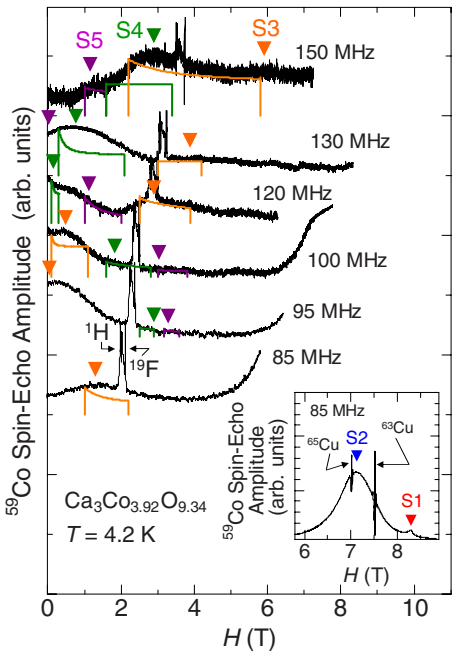

FIG. 2. (Color online) Field-swept ^{59}Co NMR spectra for $Ca_3Co_{3.92}O_{9.34}$ at 4.2 K taken at various frequencies together with the calculated AF powder patterns. Two sharp peaks observed at lower H's and higher H's are the ^{1}H and ^{19}F NMR signals, respectively, and they are caused by cellophane and polytetrafluoroethylene tapes. For instance, the former distributes at 1.996 T and the latter at 2.212 T in the data taken at 85 MHz. In the inset, H-swept ^{59}Co NMR spectrum above 5.5 T taken at 85 MHz is displayed as an expanded scale. The peaks observed at 7.532 and 7.031 T are the ^{63}Cu and ^{65}Cu NMR signals in an NMR coil, respectively.

whereas those for S1 and S2 belong to the Co in the CoO_2 layer.[21] The spin quantum number for the Co in the rock-salt layer has been claimed to be about six times larger than that for the CoO_2 layer from neutron powder diffraction and magnetic-susceptibility measurements,[27] which is consistent with relatively large $H_{\rm int}$'s for S3–S5. Furthermore, the x-ray diffraction data reveal three different Co-O bond lengths in the rock-salt layer,[28] which is compatible with our suggestion that three signals, S3–S5, come from the Co in the rock-salt layer.

On the other hand, for $[Ca_2Co_{1.3}Cu_{0.7}O_4]_{0.62}CoO_2$, a complex NMR spectrum at higher f's was observed in a wider f range compared to that for the present $Ca_3Co_{3.92}O_{9.34}$.[21] Considering the random distribution of Co and Cu in the rock-salt layer and/or quadruple-layered blocks, magnetic environments for the Co nuclei in the rock-salt layer are naturally expected to be complex, resulting in a wide distribution of $H_{\rm int}$'s. Hence, we have postulated that the NMR spectra at higher f's are assigned as signals from the Co in the rock-salt layer and the other spectra with a broad peak located from $\approx$0 to $\approx$25 MHz are assigned as signals from the Co in the CoO_2 layer similar to $Ca_3Co_{3.92}O_{9.34}$.[21]

In order to detect clearly the NMR spectra that locate at $f \leq 20$ MHz under ZF for $Ca_3Co_{3.92}O_{9.34}$, we measured the ^{59}Co NMR spectra under 6.1065 T. Figure 1(b) shows the f-swept ^{59}Co NMR spectrum at 4.2 K. Although the spectrum exhibits a broad peak around 75 MHz, the spectrum shape is well explained by the two signals, i.e., S1 and S2, and additional signals from the Cu coil. Two signals detected under H are also observed for Na_xCoO_2 that has the CoO_2 layer,[29] which also implies that they come from the Co in the CoO_2 layer.

Since the nucleus in a magnetically ordered state would experience a local magnetic field, the resonance frequency $f(f_{\rm r})$ is expressed by

$$\omega_{\rm r} = 2\pi f_{\rm r} = \gamma\sqrt{\boldsymbol{H}^2 + \boldsymbol{H}_{\rm int}^2 + 2|\boldsymbol{H}||\boldsymbol{H}_{\rm int}|\cos\,\theta}, \qquad (1)$$

where γ, $\boldsymbol{H}$, $\boldsymbol{H}_{\rm int}$, and θ are the nuclear gyromagnetic ratio, the external field, the internal field, and the angle between $\boldsymbol{H}$ and $\boldsymbol{H}_{\rm int}$, respectively. A straightforward calculation of the above equation with subsequent insertion of θ=0°, 180°, and 90° leads to simple equations

$$\omega_{{\rm r},\theta=0^\circ} = \gamma|\boldsymbol{H} + \boldsymbol{H}_{\rm int}|, \qquad (2)$$

$$\omega_{{\rm r},\theta=180^\circ} = \gamma|\boldsymbol{H} - \boldsymbol{H}_{\rm int}|, \qquad (3)$$

$$\omega_{{\rm r},\theta=90^\circ} = \gamma\sqrt{\boldsymbol{H}^2 + \boldsymbol{H}_{\rm int}^2}. \qquad (4)$$

Therefore, the magnitude and the direction of $\boldsymbol{H}_{\rm int}$ can be determined by measuring $f_{\rm r}$ as a function of H.

The H-swept ^{59}Co NMR spectra at 4.2 K taken at several f's for the randomly oriented $Ca_3Co_{3.92}O_{9.34}$ powder are shown in Fig. 2 together with the calculated AF powder patterns. It is well known that the NMR spectrum for random powders in the FM ordered state is different from that in the AF ordered state. When FM $H_{\rm int}$'s are formed, the NMR spectrum is observed at $H_0 \pm H_{\rm int}$, where H_0 is the resonance

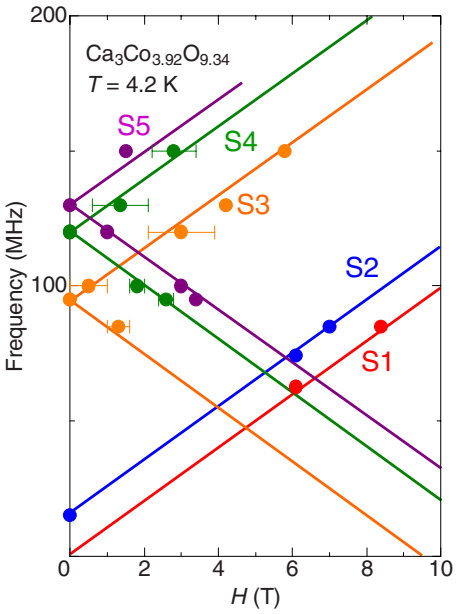

FIG. 3. (Color online) H dependence of the resonance frequency for $Ca_3Co_{3.92}O_{9.34}$ at 4.2 K. The solid lines in the figure are the results of fitting Eqs. (2) and (3) to the data, and their slope is the nuclear gyromagnetic ratio of ^{59}Co, i.e., $2\pi\times 10.054$ MHz/T. S1–S5 represent the peak positions of the NMR spectra and correspond to those in Fig. 1.

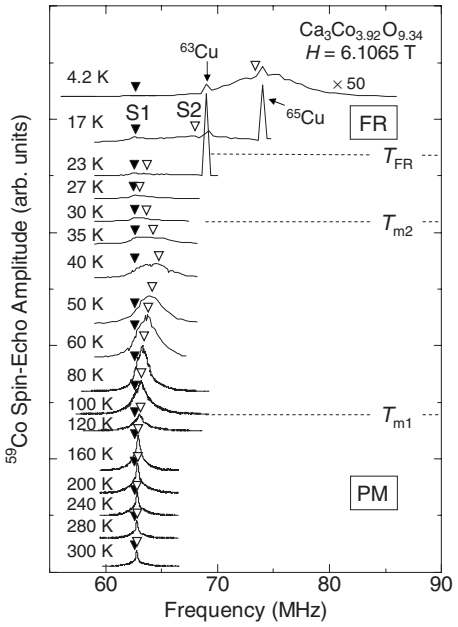

FIG. 4. Frequency-swept ^{59}Co NMR spectra for $Ca_3Co_{3.92}O_{9.34}$ measured under 6.1065 T at various T's. PM and FR denote the paramagnetic phase and the ferrimagnetic phase, respectively. The inverted triangles in the figure represent the peak positions of the spectra, and S1 and S2 correspond to those in Fig. 1(b). T_{m1}, T_{m2}, and T_{FR} are the characteristic T's (see Fig. 5 and text). The peaks observed at 68.91 and 73.82 MHz are the ^{63}Cu and ^{65}Cu NMR signals in an NMR coil, respectively. The spin-echo amplitude at 4.2 K is amplified by 50 times.

field at Knight shift $K=0$, and the sign of H_{int} depends on its direction. This is because FM moments are rotated easily to the direction of H. On the other hand, when H_{int} is AF, the NMR spectrum has a peak and a step at H_0-H_{int} ($\theta=180°$) and H_0+H_{int} ($\theta=0°$), respectively, and distributes between these fields. For the NMR spectra arising from AF H_{int}'s, the positions at higher f's were determined as the step position, whereas those at lower f's were taken as the peak position (see Fig. 2). Note here that a new broad peak at intermediate H's is attributable to the increase in a rotation of AF moments by H owing to the decrease in the anisotropic and molecular fields. However, the experimental results did not agree completely with the calculated AF powder patterns, which is probably because a simple AF order is not formed due to a complex crystal structure, e.g., a misfit between two layers. Therefore, the error bars are added in Fig. 3. The NMR spectrum taken at 85 MHz at the H range displayed in the inset of Fig. 2 did not show the powder pattern expected for AF H_{int}'s. Also, this powder pattern was not observed, even when f was decreased down to 15 MHz. Therefore, the positions of the NMR spectra showing these behaviors were determined as the peak positions.

Figure 3 shows the f_r as a function of H at 4.2 K for the same sample. It is found that there are five components, S1–S5, for the NMR spectrum at 4.2 K under ZF. Both the number and their values under ZF accord with those observed in the ZF-NMR spectrum shown in Fig. 1(a). The values of H_{int}'s under ZF are estimated as 0 T for S1, 1.5 T for S2, 9.3 T for S3, 12.7 T for S4, and 14.0 T for S5. Three of them, S3–S5, are found to agree with the two resonance conditions; that is, f_r increases (decreases) linearly with H, i.e., satisfies "two branches." On the contrary, f_r for S1 and S2 increases linearly with H, i.e., satisfies "one branch." Furthermore, the H dependence of f_r is well explained by Eq. (2) or (3). Note that the slope of the solid lines in Fig. 3 is described based on the nuclear gyromagnetic ratio of ^{59}Co, i.e., $2\pi\times 10.054$ MHz/T. These results demonstrate that AF H_{int}'s are formed in the rock-salt layer, whereas FM H_{int}'s are done partially in the CoO_2 layer. Also, it is reasonable to conclude that the values of f_r's for S1 and S2 at 6.1065 T predicted from the f_r versus H lines at 4.2 K coincide with those observed in the ^{59}Co NMR f spectrum shown in Fig. 1(b).

H_{int} at 0 K was reported to be independent of the substitution elements, the amount of the replaced elements, and the number of the rock-salt layers from μ^+SR experiments, which suggests that the IC-SDW ordered state exists in the CoO_2 layer.[20] Furthermore, since the transport properties are mainly determined by the electronic states in the CoO_2 layer, information on the local magnetic properties of this layer is critical in order to understand the physics behind the excellent thermoelectric properties of the MLCO's. Figure 4 shows the f-swept ^{59}Co NMR spectra for S1 and S2, which correspond to the signals from the CoO_2 layer of $Ca_3Co_{3.92}O_{9.34}$, measured under 6.1065 T at various T's. The NMR spectrum was clearly found to consist of two components below T_{m1} and they have asymmetric shape above T_{m1}. The physical meaning and the origin of T_{m1} are explained below. S2, whose intensity is larger than that of S1, is observed over the whole T range measured, which means that the two sites are in different proportions. The incommensu-

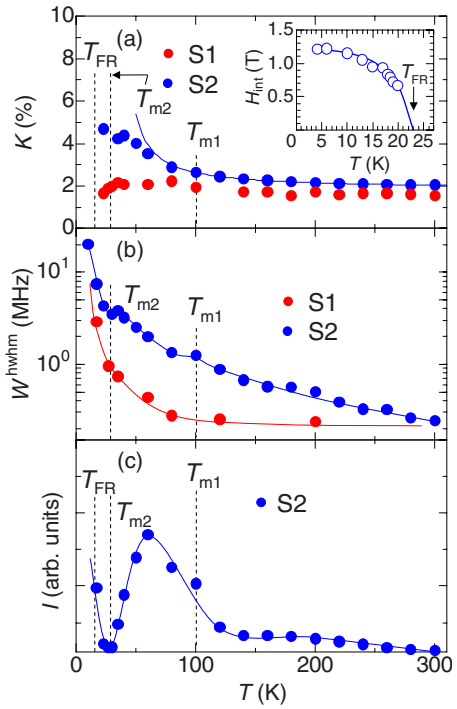

FIG. 5. (Color online) T dependences of (a) the Knight shift, (b) the half-width at half maximum, and (c) the integrated intensity of the ^{59}Co NMR spectra for $Ca_3Co_{3.92}O_{9.34}$. The inset shows the T dependence of the internal field and the solid curve is a guide to the eyes. T_{m1}, T_{m2}, and T_{FR} are the characteristic T's (see text). The solid curves in the main panel are guides to the eyes except for the result of the Curie-Weiss fitting in Fig. 5(a).

rability of the nearby rock-salt layers strongly distributes the Co electric field gradient (EFG) at the Co site in the CoO_2 layer, which may make the quadrupolar structure of the NMR spectrum very ambiguous compared to that observed for Na_xCoO_2. In order to resolve the NMR spectrum with asymmetric shape and elucidate the origin of its asymmetric shape, we measured the ^{59}Co NMR spectra for the c-axis-aligned $Ca_3Co_{3.92}O_{9.1}$ sample under the same condition; the result is explained in detail in Sec. III B. Furthermore, the peak position for S1 was almost T independent, whereas that for S2 shifted toward a lower f with increasing T, particularly below T_{m1}, due to the decrease in H_{int} with T. A similar behavior was also observed for $[Ca_2Co_{1.3}Cu_{0.7}O_4]_{0.62}CoO_2$.[21] On the other hand, the NMR signals, corresponding to S3–S5, were not observed in this measurement condition, probably because the nuclei spin-spin relaxation time (T_2) is too short to be observable due to the magnetic interaction between the Co ions in the rock-salt layer.

In order to clarify the changes in the S1 and S2 signals with varying T, the T dependences of the ^{59}Co Knight shift K and H_{int} for $Ca_3Co_{3.92}O_{9.34}$ are plotted in Fig. 5(a). Here, we define K as $K=(f_r-f_0)/f_0$, where $f_0=\gamma H/2\pi$ with $\gamma=2\pi \times 10.054$ MHz/T and $H=6.1065$ T. K for S1 (K_{S1}) was about 1.8%, while K_{S2} showed a T dependence. K_{S2} above $\approx$100 K, expressed as T_{m1}, obeyed the Curie-Weiss law, $K_{S2}=1.84+50.6/(T-35.7)$% [a solid curve in Fig. 5(a)]. The fairly good fit and the positive Weiss temperature of 35.7 K with quite small error indicate a FM interaction between the Co ions at the Co sites that are responsible for S2. This result is consistent with the conclusion derived from the relationship between f_r and H. The $K_{S2}(T)$ curve exhibited a plateau at $\approx$40 K. Also, this curve suggests the presence of H_{int} and the $H_{int}(T)$ curve increased significantly below 23 K(T_{FR}), below which the FR order appears, as is clearly seen in the inset of Fig. 5(a). Here, $H_{int}=2\pi|f_r-f_0|/\gamma$. Similar T dependence of K_{S1}, K_{S2}, and H_{int} has also been observed for $[Ca_2Co_{1.3}Cu_{0.7}O_4]_{0.62}CoO_2$.[21]

Figure 5(b) shows the T dependence of the half-width at half maximum (W^{hwhm}) of the ^{59}Co NMR spectra measured under 6.1065 T for $Ca_3Co_{3.92}O_{9.34}$. W^{hwhm} is known to depend on the field inhomogeneities arising from the variation in the demagnetizing field within a given particle and between different particles, the nuclear-nuclear dipolar interaction, and the time-dependent electron-nuclear magnetic interaction. Basically, W^{hwhm} for this compound plotted in Fig. 5(b) is determined by fitting the NMR spectrum with a combination of two Gaussian functions. W^{hwhm}'s for S1 and S2 (W_{S1}^{hwhm} and W_{S2}^{hwhm}) are found to increase with decreasing T. In particular, the $W_{S2}^{hwhm}(T)$ curve changes its slope at T_{m1} and T_{m2}; that is, the slope becomes steeper with decreasing T. Note that it was difficult to estimate W_{S1}^{hwhm} for every T point due to the weak intensity of the S1 signal.

Figure 5(c) shows the T dependence of the integrated intensity I for S2 (I_{S2}) for $Ca_3Co_{3.92}O_{9.34}$. In the paramagnetic (PM) phase, the change in I with varying T was small. Upon cooling, I increased gradually and exhibited a peak; then decreased and finally increased again below T_{m2}. The changes in I at T_{m1} and T_{m2} with varying T are likely to correlate with the T variations in K and/or W^{hwhm}. However, although T_2, which determines I_{S2}, would be very short, particularly below $\approx$60 K due to the magnetic order, the T dependences of the NMR parameters (K_{S2}, W_{S2}^{hwhm}, and I_{S2}) are still not fully explained at present.

B. c-axis-aligned $Ca_3Co_{3.92}O_{9.1}$

The ^{59}Co NMR spectrum in the FR state for the c-axis-aligned sample of $Ca_3Co_{3.92}O_{9.1}$ under ZF is shown in Fig. 6(a). As is clear from this figure, the spectrum at $f \geq 40$ MHz consisted of mainly three components. In the ^{59}Co NMR measurements under 6.1065 T at 4.2 K, we also observed two sets of ^{59}Co NMR spectra, as in the case of $Ca_3Co_{3.92}O_{9.34}$ [see Fig. 6(b)]. The S1 and S2 signals observed under 6.1065 T are located at $f \leq 40$ MHz under ZF. These results also demonstrate the existence of the five nonequivalent Co sites. Because the crystal structure of $Ca_3Co_{3.92}O_{9.34-\delta}$ does not change significantly with δ, the NMR lines at higher f's are assigned as signals from the Co in the rock-salt layer and the others are assigned as signals from the Co in the CoO_2 layer.

The H-swept ^{59}Co NMR spectra at 4.2 K taken at various f's were obtained for the c-axis-aligned $Ca_3Co_{3.92}O_{9.1}$ sample for $H\|$ the c axis. We observed the ^{59}Co NMR spectrum with a few components at each f. Fundamentally, the position of the signals S1–S5 was determined as the peak position. The NMR spectrum for S3 was broad, which is due

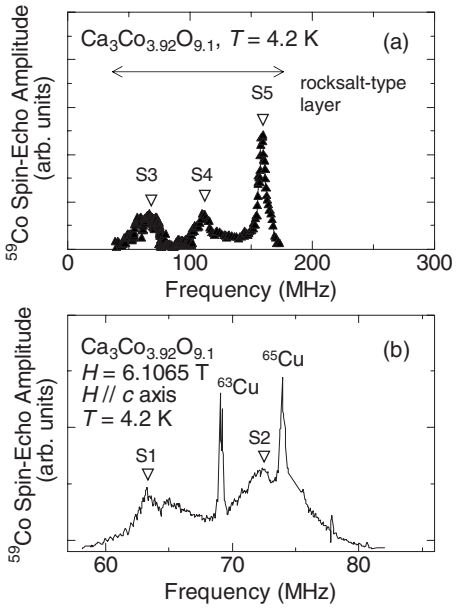

FIG. 6. Frequency-swept ^{59}Co NMR spectra for the c-axis-aligned sample of $Ca_3Co_{3.92}O_{9.1}$ at 4.2 K under (a) ZF and (b) 6.1065 T for $H\|$ the c axis. S1–S5 represent the peak positions of the NMR spectra. The solid line in Fig. 6(a) is a guide to the eyes. The peaks observed at 68.91 and 73.82 MHz in Fig. 6(b) are the ^{63}Cu and ^{65}Cu NMR signals in an NMR coil, respectively. The NMR line at 77.8 MHz is from a radio FM broadcast.

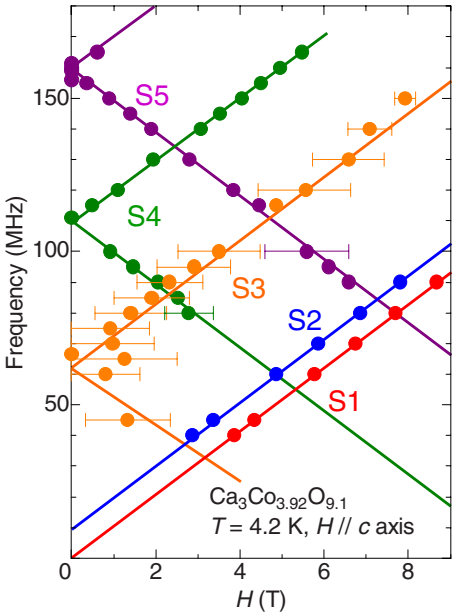

FIG. 7. (Color online) H dependence of the resonance frequency for the c-axis-aligned sample of $Ca_3Co_{3.92}O_{9.1}$ at 4.2 K for $H\|$ the c axis. The solid lines in the figure are the results of fitting Eqs. (2) and (3) to the data, and their slope is the nuclear gyromagnetic ratio of ^{59}Co, i.e., $2\pi\times 10.054$ MHz/T. S1–S5 correspond to those in Fig. 6.

to the electric quadrupole interaction. The quadrupolar frequency (ν_Q) for S3 was found to be $\approx$3 MHz. As for the S3 signal, we plotted the positions of central lines in Fig. 7. $f_{r\|}$ for this sample is plotted as a function of H in Fig. 7. The values of H_{int}'s under ZF are estimated as 0, 1.0, 5.9, 12.4, and 15.9 T for S1, S2, S3, S4, and S5, respectively. The resonance conditions of $f_{r\|}$ for S1–S5 were the same as those for $Ca_3Co_{3.92}O_{9.34}$.

We also measured the H-swept ^{59}Co NMR spectra at 4.2 K and various f's for $H\perp$ the c axis. The NMR spectrum with a few components was observed at each f independent of the direction of H. Although the NMR spectra measured for $H\perp$ the c axis were broad compared to those for $H\|$ the c axis, we roughly determined the peak positions, as in the case of $H\|$ the c axis. As displayed in Fig. 8, the H dependence of $f_{r\perp}$ followed Eq. (4). The values of H_{int}'s under ZF for $H\perp$ the c axis are naturally the same as those for $H\|$ the c axis. By taking advantage of the orientation, the conclusion that the direction of H_{int} is along the c axis can be derived from the results plotted in Figs. 7 and 8.

Figures 9 and 10 show the T dependence of the f-swept ^{59}Co NMR spectra for S1 and S2, which correspond to the signals from the CoO_2 layer of the c-axis-aligned $Ca_3Co_{3.92}O_{9.1}$ sample, measured under 6.1065 T for $H\|$ the c axis and $H\perp$ the c axis, respectively. The ^{59}Co NMR spectrum at 120 K is displayed in the inset as an expanded scale together with that of the randomly oriented $Ca_3Co_{3.92}O_{9.34}$ sample. The clear peak structure attests the high quality of the sample. The I=7/2 nuclear spin of ^{59}Co senses the magnetic properties of the Co site and couples through its nuclear quadrupole moment to the EFG tensor created by its charge environment. The ^{59}Co NMR spectrum for $H\|$ the c axis is the most typical one for the two sites for which the c axis is the principal axis of the EFG. This result indicates that the NMR spectrum observed under 6.1065 T for these samples consists of the signals from S1 and S2 even in the PM phase, although the NMR spectrum for S2 overlapped that for S1 at

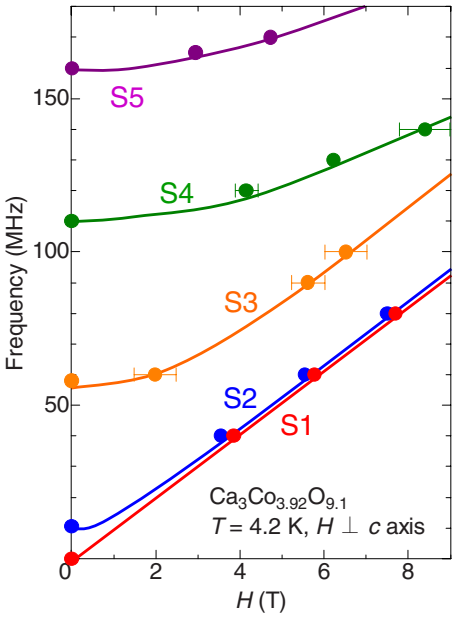

FIG. 8. (Color online) H dependence of the resonance frequency for the c-axis-aligned sample of $Ca_3Co_{3.92}O_{9.1}$ at 4.2 K for $H\perp$ the c axis. The solid curves in the figure are the results of fitting Eq. (4) to the data. S1–S5 correspond to those in Fig. 6.

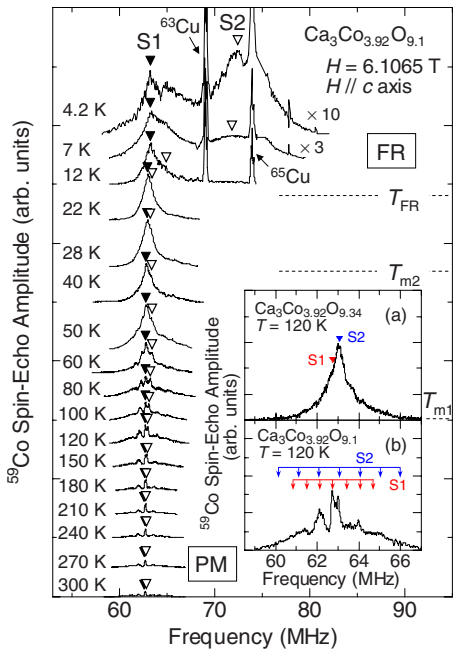

FIG. 9. (Color online) Frequency-swept ^{59}Co NMR spectra for the c-axis-aligned sample of $Ca_3Co_{3.92}O_{9.1}$ measured under 6.1065 T at various T's for $H\|$ the c axis. The inverted triangles in the figure represent the peak positions of the central lines split by the electric quadrupole interaction. PM, FR, T_{m1}, T_{m2}, and T_{FR} have the same meaning as those in Fig. 4 (see Fig. 11 and text). The peaks observed at 68.91 and 73.82 MHz are the ^{63}Cu and ^{65}Cu NMR signals in an NMR coil, respectively. The sharp line at 77.8 MHz is from a radio FM broadcast. The spin-echo amplitudes at 4.2 and 7 K are amplified by 10 times and 3 times, respectively. The inset shows f-swept ^{59}Co NMR spectra for (a) the randomly oriented polycrystalline $Ca_3Co_{3.92}O_{9.34}$ sample and (b) the c-axis-aligned $Ca_3Co_{3.92}O_{9.1}$ sample measured under 6.1065 T at 120 K. In the latter compound, H is applied parallel to the c axis. The arrows denote the ^{59}Co NMR lines split by the electric quadrupole interaction.

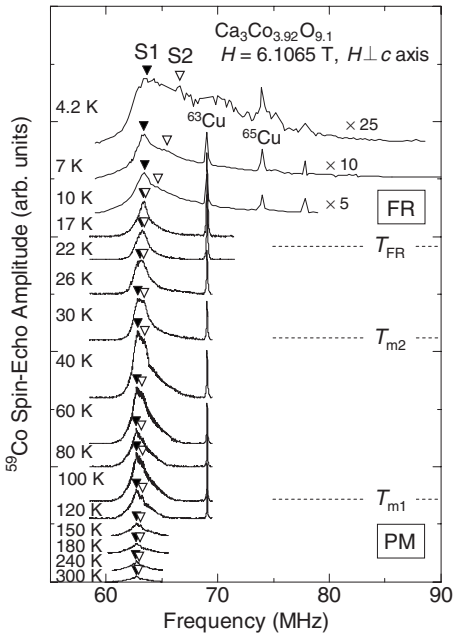

FIG. 10. Frequency-swept ^{59}Co NMR spectra for the c-axis-aligned sample of $Ca_3Co_{3.92}O_{9.1}$ measured under 6.1065 T at various T's for $H\perp$ the c axis. The inverted triangles in the figure represent the peak positions of the spectra. PM, FR, T_{m1}, T_{m2}, and T_{FR} have the same meaning as those in Fig. 4 (see Fig. 12 and text). The peaks observed at 68.91 and 73.82 MHz are the ^{63}Cu and ^{65}Cu NMR signals in an NMR coil, respectively. The sharp line at 77.8 MHz is from a radio FM broadcast. The spin-echo amplitudes at 4.2, 7, and 10 K are amplified by 25 times, 10 times, and 5 times, respectively.

around room temperature. ν_Q and the asymmetric parameter η for S1 are evaluated to be ≈ 1 MHz and 0.20, respectively. The ^{59}Co NMR f under ZF generally depends on both ν_Q and η, and their estimated values rule out the possibility that the NMR spectrum under 6.1065 T consisting of two signals comes from two components among S3–S5 assuming that the charge distribution around cobalt nucleus remains unaltered with varying T because of no structural phase transition. As T is lowered, the quadrupole singularities spread and Lorentzian NMR spectra were observed. On the other hand, the crystallites are almost random for $H\perp$ the c axis, resulting in powder spectra (see Fig. 10). Hence, although the splitting due to the electric quadrupole interaction was ambiguous compared to that for $H\|$ the c axis, the spectrum consisting of the S1 and S2 signals was observed.

Figures 11 and 12 show the T dependences of K, H_{int}, and I for the c-axis-aligned sample of $Ca_3Co_{3.92}O_{9.1}$ for $H\|$ the c axis and $H\perp$ the c axis, respectively. The K_{S1} measured in both conditions was almost T independent ($\approx 3.5\%$), but K_{S2} was dependent on T. The T dependence of K_{S2}, particularly in the T range above T_{m1}, was fitted by a Curie-Weiss formula, $K_{S2}=1.77+46.6/(T-41.5)\%$, which is shown in Fig. 11(a) as the solid curve. H_{int} for S2 was found to be ≈ 1 T at 4.2 K and decreased drastically upon heating to T_{FR}. As can be seen from Fig. 12(b), although the change in the I versus T curve for $H\perp$ the c axis was less clear than that for $H\|$ the c axis, an increase in I below T_{m2} was commonly observed. The T variations in K, H_{int}, and I corresponding to S2 for $H\|$ the c axis seem to exhibit changes at T_{m1}, T_{m2}, and T_{FR} as in the case of $Ca_3Co_{3.92}O_{9.34}$.

Furthermore, the anisotropy of K was smaller than that of the magnetic susceptibility χ. For instance, the ratio χ_c/χ_{ab} has been reported to be about 2 at 100 K for the c-axis-aligned $[Ca_2CoO_{3-\delta}]_{0.62}CoO_2$ sample prepared by applying magnetic alignment in which χ_c and χ_{ab} are the magnetic susceptibility when H is applied parallel to the c axis and the ab plane, respectively.[30] The small anisotropy of K implies that the macroscopic magnetism of the MLCO's with a triple subsystem is dominated by the local magnetic properties coming from the Co in the rock-salt layer. However, only AF H_{int}'s are formed in the rock-salt layer. Therefore, the magnetic interaction in the CoO_2 layer is not negligibly weak to stabilize the FR state. Furthermore, T_{FR} depended on the oxygen content and decreased with increasing δ [see the insets in Figs. 5(a) and 11(a)]. This behavior is probably due to the smaller concentration of holes in the Co^{4+}/Co^{3+} couple.

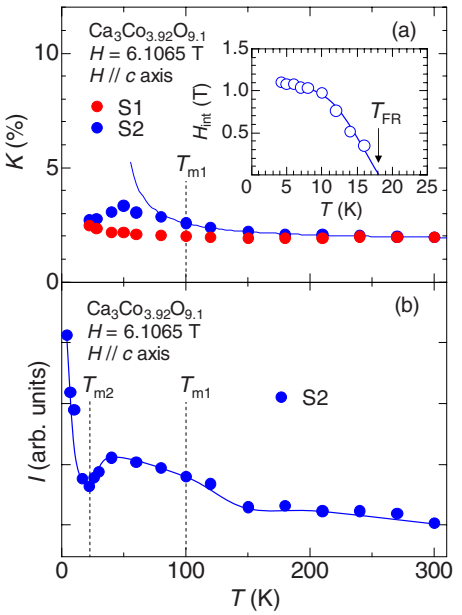

FIG. 11. (Color online) T dependences of (a) the ^{59}Co Knight shift and (b) the integrated intensity for the c-axis-aligned sample of $Ca_3Co_{3.92}O_{9.1}$ for $H\|$ the c axis. The inset shows the T dependence of the internal field. The solid curve in the main panel of Fig. 11(a) shows the result of the Curie-Weiss fitting and the other curves are guides to the eyes. T_{m1}, T_{m2}, and T_{FR} have the same meaning as those in Fig. 4.

C. Randomly oriented polycrystalline $Ca_3Co_{3.92}O_9$ with large oxygen vacancy

The existence of five nonequivalent Co sites with different H_{int}'s at 4.2 K was also confirmed by the ^{59}Co NMR measurements under ZF and 6.1065 T (see Fig. 13), as in the cases of $Ca_3Co_{3.92}O_{9.34}$ and $Ca_3Co_{3.92}O_{9.1}$. Also, the intensity ratio of the S1 and S2 signals was found to depend strongly on the oxygen content in the MLCO's with a triple subsystem in comparison with Figs. 1(b), 6(b), and 13(b). In other words, the relative intensity of the S1 signal increased with decreasing oxygen content.

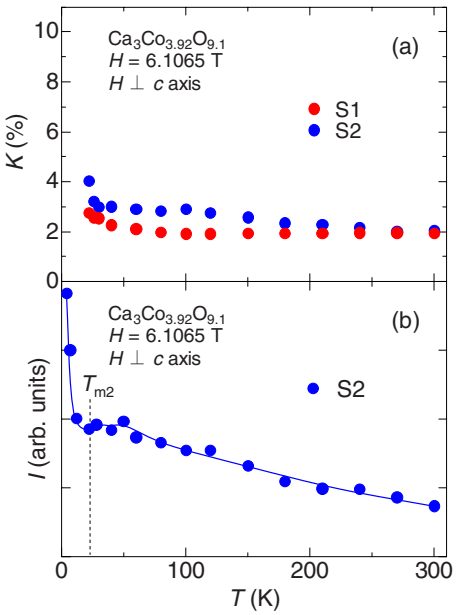

FIG. 12. (Color online) T dependences of (a) the ^{59}Co Knight shift and (b) the integrated intensity for the c-axis-aligned sample of $Ca_3Co_{3.92}O_{9.1}$ for $H\perp$ the c axis. The solid curve in Fig. 12(b) is a guide to the eyes. T_{m2} is the temperature below which I increased rapidly.

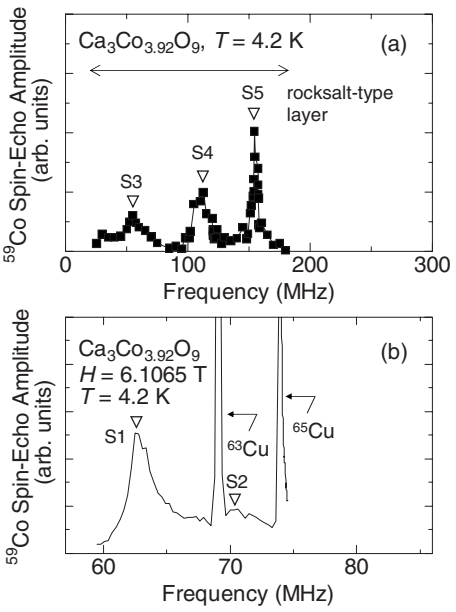

FIG. 13. Frequency-swept ^{59}Co NMR spectra for $Ca_3Co_{3.92}O_9$ at 4.2 K under (a) ZF and (b) 6.1065 T. S1–S5 represent the peak positions of the NMR spectra. The solid line in Fig. 13(a) is a guide to the eyes. The peaks observed at 68.91 and 73.82 MHz in Fig. 13(b) are the ^{63}Cu and ^{65}Cu NMR signals in an NMR coil, respectively.

Figure 14 shows the f-swept ^{59}Co NMR spectra measured under 6.1065 T at various T's for S1 and S2, which correspond to the signals from the CoO_2 layer of $Ca_3Co_{3.92}O_9$. The quadrupole-broadened NMR spectrum consists of two components, as in the cases of $Ca_3Co_{3.92}O_{9.34}$, $Ca_3Co_{3.92}O_{9.1}$, and $[Ca_2Co_{1.3}Cu_{0.7}O_4]_{0.62}CoO_2$. Here, it is worth emphasizing that the NMR spectrum was governed by the component corresponding to S1 whose K exhibited almost T-independent behavior, which is an opposite trend compared to $Ca_3Co_{3.92}O_{9.34}$ with almost no oxygen vacancy. This result indicates that the dominant interaction affecting the local magnetism in the CoO_2 layer at lower T's in the MLCO's with a triple subsystem depends strongly on the oxygen content, i.e., the carrier concentration.

Figure 15(a) shows the T dependence of W_{S1}^{hwhm} of the NMR spectra measured under 6.1065 T for $Ca_3Co_{3.92}O_9$. W^{hwhm} of the NMR spectrum for this material was analyzed by fitting a single Gaussian function to the data because of a dominant contribution of S1 to the NMR spectrum as already mentioned above. W^{hwhm} for S1 increased below T_{m1} and exhibited a plateau at $\approx$50 K. When further cooled, W_{S1}^{hwhm} increased again below $\approx T_{m2}$. Two characteristic temperatures T_{m1} and T_{m2} below which W_{S1}^{hwhm} increased were found to correlate with the T at which I_{S1} showed the peculiar changes as in the case of $Ca_3Co_{3.92}O_{9.34}$ [see Fig. 15(b)].

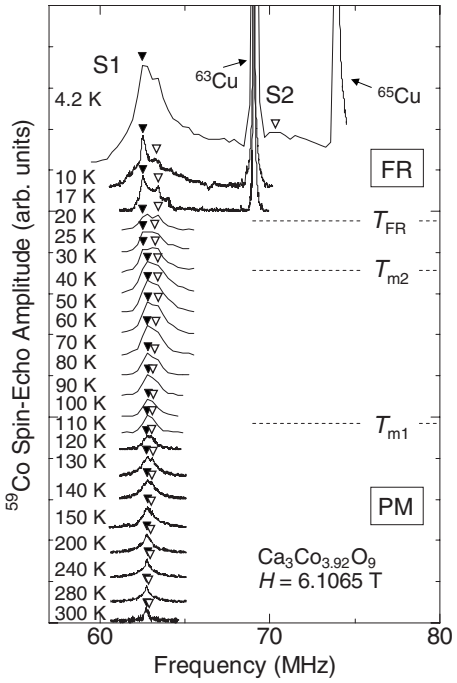

FIG. 14. Frequency-swept ^{59}Co NMR spectra for $Ca_3Co_{3.92}O_9$ measured under 6.1065 T at various T's. The inverted triangles in the figure represent the peak positions of the spectra. PM, FR, T_{m1}, T_{m2}, and T_{FR} have the same meaning as those in Fig. 4 (see Fig. 15 and text). The peaks observed at 68.91 and 73.82 MHz are the ^{63}Cu and ^{65}Cu NMR signals in an NMR coil, respectively.

IV. DISCUSSION

A. Origin of the magnetism

By a systematic study of ^{59}Co NMR measurements for the MLCO's, the ^{59}Co NMR spectrum coming from the Co in the CoO_2 layer was found to consist of mainly two lines. One

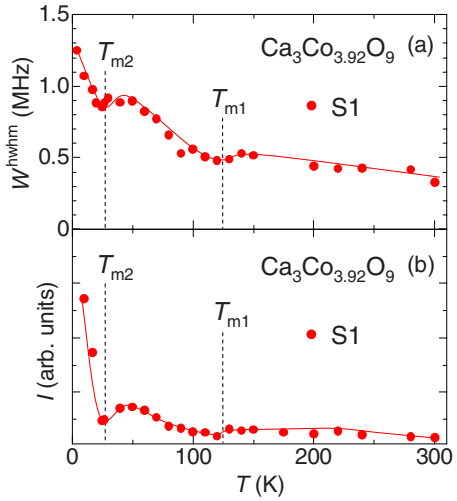

FIG. 15. (Color online) T dependences of (a) the half-width at half maximum and (b) the integrated intensity of the ^{59}Co NMR spectrum corresponding to the S1 signal for $Ca_3Co_{3.92}O_9$. T_{m1} and T_{m2} have the same meaning as those in Fig. 4. The solid curves are guides to the eyes.

of them, S1, has a zero H_{int} under ZF and the other, S2, has a nonzero H_{int} under ZF (FM H_{int}'s). This behavior is unconventional because two of the H_{int}'s exist simultaneously in a single layer even consisting of one crystallographically equivalent Co site. There may be a few scenarios to explain these experimental findings. One is that there are two nonequivalent sites in a single uniform phase, wherein two different electronic states around equivalent cobalt nuclei exist, for example, due to a charge-ordered state. Another is more realistic, i.e., a view based on a separation between two phases. Quite recently, the phase separation between the charge-ordered insulating state and the PM metallic state has been claimed by photoemission spectroscopy experiments.[31] According to their measurements, holes are localized regularly in the former state, while they are itinerant and distributed uniformly in the latter state.[31] Since EFG depends sensitively on the charge distribution around the nucleus, any change in the EFG value is related to either the structural phase change or the change in electronic state. When a charge-ordered state is realized in the MLCO's, ν_Q changes with varying T. However, the almost constant behavior of ν_Q^c for S1 and S2 evidences the absence of any charge ordering at least down to T_{m2}. In our NMR experiments, however, the coexistence of the SDW and FM order would be proposed, the detail of which is discussed as follows. The intensity ratio of the S1 and S2 signals depended strongly on the oxygen content in MLCO's with a triple subsystem. The NMR spectrum for S1 whose K showed almost T-independent behavior is predominant in the sample with the large δ. The NMR spectrum S1 for $Ca_3Co_{3.92}O_9$ below 17 K had a characteristic triangular shape, which is similar to that expected for a typical SDW ordered state. Therefore, we verify the possibility of the SDW state. The NMR shape function F in the SDW ordered state is expressed as

$$F \propto \ln(1+\sqrt{1-x^2})/|x|, \tag{5}$$

where $x=(H-\omega/\gamma)/(H_{int})_{max}$ and $(H_{int})_{max}$ is the respective maximum amplitude of the internal field.[32] The NMR spectrum at 4.2 K for $Ca_3Co_{3.92}O_9$ could be roughly fitted by this equation as seen in Fig. 16(a). Because the NMR spectrum for S1 above 10 K overlapped that for S2, we fitted the NMR spectrum using a combination of Eq. (5) and a Gaussian function. As can be seen from Fig. 16(b), the NMR spectrum at 10 K with two components seems to be explained by these two functions. The values of $(H_{int})_{max}$ were estimated to be 0.27, 0.20, and 0.10 T at 4.2, 10, and 17 K, respectively. Considering both the μ^+SR and the present NMR data, the SDW ordered state is likely realized in the CoO_2 layer, particularly for MLCO's with a large δ.

Interestingly, the coexistence of coherent electrons and incoherent ones for the MLCO's has been argued by photoemission spectroscopy experiments.[33] The enhancement of ρ with decreasing T in the IC-SDW ordered state is more distinct with increasing δ,[24] which implies that the electrons for S1 have an incoherent nature and those for S2 have a coherent nature. On the other hand, the partial electronic states corresponding to the rock-salt layer may be formed by incoherent electrons because the electrical conductivity in this layer is insulating.

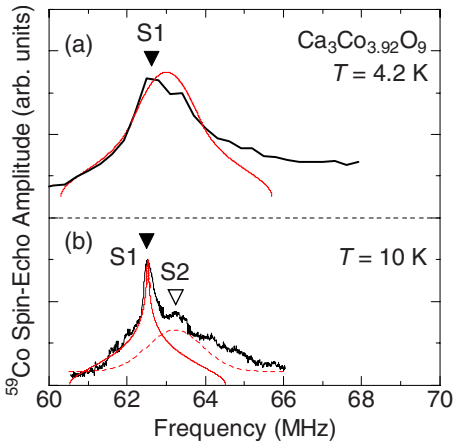

FIG. 16. (Color online) ^{59}Co NMR spectra for $Ca_3Co_{3.92}O_9$ measured under 6.1065 T at (a) 4.2 K and (b) 10 K. The solid and dashed curves are the result of fitting Eq. (5) and a Gaussian function to the data, respectively. The former curves represent $F(x)$ smeared over a range of 1/5 and 1/65 of $(H_{int})_{max}$ at 4.2 and 10 K, respectively.

For the same sample used in the μ^+SR experiments, i.e., the c-axis-aligned $Ca_3Co_4O_{9.1}$ sample, the T dependences of H_{int}, K, W^{hwhm}, and I for S2, whose signal shows the positive Weiss T and FM H_{int}'s, are rather likely to correlate with the phase diagram determined by the μ^+SR measurements. Therefore, the magnetic nature detected by means of this technique may be mostly due to the T variation in the magnetism with the FM interaction. However, the existence of SDW order in the MLCO's with a triple subsystem is not necessarily denied because we observed an NMR spectrum in which both the existence of the SDW and FM orders could possibly be inferred; the degree of their competition would be controlled by the oxygen content in $Ca_3Co_{3.92}O_{9.34-\delta}$.

The appearance and stability of the SDW phase have been theoretically discussed by the Hubbard model within a mean-field approximation using parameters such as the electron filling, the Hubbard on-site repulsion, and the nearest-neighbor hopping amplitude.[34,35] Based on the phase diagram proposed by the extended Hubbard model on a triangular lattice, an increase in the on-site repulsion leads to a competition between the SDW and FM order.[36] The electronic specific-heat coefficient γ of $Ca_3Co_4O_9$ has been reported to be as large as $\approx$90 mJ/mol K^2, which is about two times larger than γ of $NaCo_2O_4$,[37,38] indicating $Ca_3Co_4O_9$ is a strongly correlated electron material. Therefore, the competition can be interpreted by the strong correlation between 3d electrons. In this model, the FM order is suppressed with increasing electron filling and the boundary between the SDW and FM order is almost electron-filling independent.[36] The trend that an increase in the electron filling leads SDW order can be accounted for in the model calculation provided there is a decrease in first-neighbor repulsion with increasing δ. Also, the development of SDW order with decreasing n coincides with the phase diagram for Na_xCoO_2, in which the onset T of the SDW order observed for x=0.75 increases with x.[3] The ground state for the CoO_2 layer in $Ca_3Co_{3.92}O_{9.34-\delta}$ may be summarized with the phase diagram of Fig. 17.

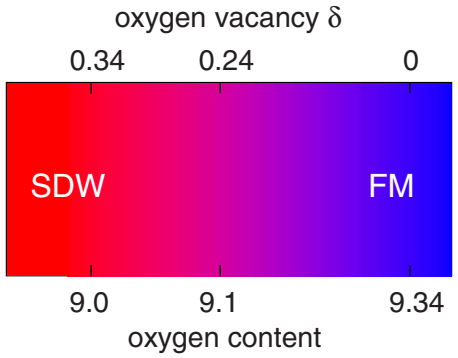

FIG. 17. (Color online) Schematic phase diagram of the CoO_2 layer in $Ca_3Co_{3.92}O_{9.34-\delta}$ proposed by the present NMR measurements.

Next, we discuss briefly the magnetic nature at T_{m1}, T_{m2}, and T_{FR}. Below T_{m1}, the K_{S2} versus T curve deviated from the Curie-Weiss law and bent downward. And also, the asymmetry of a weak transverse field μ^+SR spectrum that is proportional to the volume fraction of a PM phase decreased below T_{m1}. These results suggest that a magnetic order develops below T_{m1}. Because the values of K_{S2} below T_{m1} was smaller than those expected from the Curie-Weiss law, a short-range AF order coming from an interplane interaction is thought to develop below T_{m1}. On the other hand, the origin of the change in K at T_{m2} is still unclear for the samples of $Ca_3Co_{3.92}O_{9.34}$ and $Ca_3Co_{3.92}O_{9.1}$. However, we can exclude the possibility that T_{m2} is a competition T as reported for the rare-earth iron garnets. This is because a clear hysteretic loop is observed only below T_{FR}. In addition, an anomalous enhancement in the Co-Co correlation in the CoO_2 layer has been reported to occur at T_{m2}.[39] For these samples, the short-range FM order in the CoO_2 layer may develop below T_{m2}, which may be caused by the frustration due to a 2D triangular lattice and the disorder. Because the integrated intensity for S2 exhibited a minimum at around T_{m2}, the great majority of magnetic moments would be already aligned ferromagnetically at this temperature. In contrast to these interpretations, the characteristic temperatures T_{m1} and T_{m2} observed in $Ca_3Co_{3.92}O_9$ may correspond to the onset T of the short-range IC-SDW order and the long-range one, respectively, since an analysis of the NMR shape for S1 at low T below which the S1 and S2 signals are distinguishable indicates the presence of a SDW order.

B. Magnetism and transport properties

An increase in δ in $Ca_3Co_{3.92}O_{9.34-\delta}$ may increase both S and ρ due to a decrease in the carrier concentration (n). This behavior can be understood by a simple model assuming a parabolic band, in which both of them vary monotonically as a function of n,[40] i.e., they increase with decreasing n. In the framework of the band picture, electrons inside the energy range of a few k_BT in width centered at the chemical potential are attributable to the transport properties, where k_B is the Boltzmann constant. Quite recently, it has been revealed that the density of states (DOS) that arises from the coherent electrons located at the lower binding-energy region, while

the DOS that arises from the incoherent electrons is at the higher binding-energy region.[33] Therefore, the contribution of the DOS with a coherent nature near the Fermi level E_F dominates the transport properties at lower T's. In particular, the narrow band with a sharp slope in the vicinity of E_F, which is caused by the strong electron correlation, gives a steep increase in S at lower T's. With increasing T, the incoherent electrons, in addition to the coherent ones, are also attributable to S. As already mentioned in the introduction, theoretical work has proposed the importance of the degeneracy of spins and orbitals of the 3d electrons of the Co ions on the enhancement of S.[22] In the MLCO's investigated in this work, the magnetic order is completed at low T, which means that the freedom of spins of the 3d electrons is not frozen at higher T's. Furthermore, $Ca_3Co_{3.92}O_{9.34}$ exhibits a spin-state transition at around 380 K.[19] However, the spin state of Co^{3+} still remains in the low-spin (LS) state and that of Co^{4+} is changed from the LS to intermediate-spin (IS) state with increasing T. Because the IS state of Co^{4+} has higher degeneracy than the LS state of Co^{4+}, this spin-state transition enhances the entropy of spins and orbitals of the 3d electrons, resulting in a large S at high T.

In $Ca_3Co_{3.92}O_{9.34-\delta}$, the number of electrons with coherent/incoherent nature in the CoO_2 layer would be changed by controlling the oxygen content, which highlights the role of each electron to the transport properties. S and ρ increase with δ in the whole T range below 300 K.[23] This is probably because the slope of the DOS near E_F does not significantly depend on δ, in addition to a decrease in a finite DOS with increasing δ. Although S of $Ca_3Co_{3.92}O_{9.34-\delta}$ at high T would also increase with δ because of the contribution of the incoherent electrons, the coherent electrons are responsible for the metallic conductivity. Provided that a finite DOS in the vicinity of E_F becomes steeper with decreasing δ, the δ dependence of the $S(T)$ curve is exciting; that is, the enhancement of S surpasses the increase in ρ with increasing δ up to the energy range where the coherent electrons are attributable to the transport properties. Furthermore, a large S will still remain at high T by the contribution of the incoherent electrons. If the increase in S is larger than that in ρ at high T, the good thermoelectric performance will also be realized. Therefore, in either side, in order to realize excellent thermoelectric performance, both a narrow band with a strongly energy-dependent DOS being formed by the electrons with coherent nature in the vicinity of E_F and a large entropy of spins and orbitals of the incoherent electrons are concluded to be needed.

V. CONCLUSION

^{59}Co NMR measurements were conducted to study the local magnetic properties of misfit layered cobalt dioxides with randomly oriented polycrystalline $Ca_3Co_{3.92}O_{9.34}$ and $Ca_3Co_{3.92}O_9$ samples, together with a c-axis-aligned sample of $Ca_3Co_{3.92}O_{9.1}$ of high quality. We successfully observed the ^{59}Co NMR spectra corresponding to signals from the Co both in the CoO_2 layer and the rock-salt layer and clarified the magnetic interactions that give rise to various magnetic orders. Specifically, the separation between two phases was found in the CoO_2 layer consisting of a crystallographically unique Co site and the degree of competition between them depended on the oxygen contents in misfit layered cobalt dioxides with a triple subsystem. The coexistence of both coherent and incoherent electrons in the conducting layer is considered to be one of the origins of the excellent thermoelectric performance for misfit layered cobalt dioxides.

ACKNOWLEDGMENTS

This study was supported by the Grant-in-Aid for Scientific Research (Grant No. 19340097) from the Japan Society for the Promotion of Science and by the Grant-in-Aid for Scientific Research (Grant No. 19014007) from the Ministry of Education, Culture, Sports, Science, and Technology of Japan. We thank J. B. Goodenough and J. S. Zhou for fruitful discussions. T.T. gratefully acknowledges the support by the Grant-in-Aid for Scientific Research (Grant No. 21740251) from the Japan Society for the Promotion of Science, the support by the Nagoya University Science Foundation, the support by the Research Foundation for the Electrotechnology of Chubu, and the support by the Sasakawa Scientific Research Grant from the Japan Science Society.

*takami.tsuyoshi@g.mbox.nagoya-u.ac.jp

[1] I. Terasaki, Y. Sasago, and K. Uchinokura, Phys. Rev. B **56**, R12685 (1997).
[2] K. Takada, H. Sakurai, E. Takayama-Muromachi, F. Izumi, R. A. Dilannian, and T. Sasaki, Nature (London) **422**, 53 (2003).
[3] M. L. Foo, Y. Wang, S. Watauchi, H. W. Zandbergen, T. He, R. J. Cava, and N. P. Ong, Phys. Rev. Lett. **92**, 247001 (2004).
[4] J. Sugiyama, H. Itahara, J. H. Brewer, E. J. Ansaldo, T. Motohashi, M. Karppinen, and H. Yamauchi, Phys. Rev. B **67**, 214420 (2003).
[5] T. Takami, H. Ikuta, and U. Mizutani, Trans. Mater. Res. Soc. Jpn. **29**, 2777 (2004).
[6] H. Fujishiro, Y. Fujine, Y. Kashiwada, M. Ikebe, and J. Hejtmanek, Proceedings of the 22nd International Conference on Thermoelectrics (ICT2003), 2003 (unpublished) p. 235.
[7] J. Androulakis, P. Migiakis, and J. Giapintzakis, Appl. Phys. Lett. **84**, 1099 (2004).
[8] J. Sugiyama, H. Nozaki, J. H. Brewer, E. J. Ansaldo, T. Takami, H. Ikuta, and U. Mizutani, Phys. Rev. B **72**, 064418 (2005).
[9] J. Sugiyama, H. Nozaki, Y. Ikedo, K. Mukai, D. Andreica, A. Amato, J. H. Brewer, E. J. Ansaldo, G. D. Morris, T. Takami, and H. Ikuta, Phys. Rev. Lett. **96**, 197206 (2006).
[10] H. Nozaki, M. Janoschek, B. Roessli, J. Sugiyama, L. Keller, J. H. Brewer, E. J. Ansaldo, G. D. Morris, T. Takami, and H. Ikuta, Phys. Rev. B **76**, 014402 (2007).
[11] H. Kageyama, K. Yoshimura, K. Kosuge, H. Mitamura, and T. Goto, J. Phys. Soc. Jpn. **66**, 1607 (1997).
[12] S. Aasland, H. Fjellvåg, and B. Hauback, Solid State Commun.

101, 187 (1997).
[13] T. Takami, H. Nozaki, J. Sugiyama, and H. Ikuta, J. Magn. Magn. Mater. **310**, e438 (2007).
[14] M. Mikami, R. Funahashi, M. Yoshimura, Y. Mori, and T. Sasaki, J. Appl. Phys. **94**, 6579 (2003).
[15] T. Takami, H. Ikuta, and U. Mizutani, Jpn. J. Appl. Phys., Part 1 **43**, 8208 (2004).
[16] A. C. Masset, C. Michel, A. Maignan, M. Hervieu, O. Toulemonde, F. Studer, B. Raveau, and J. Hejtmanek, Phys. Rev. B **62**, 166 (2000).
[17] Y. Miyazaki, T. Miura, Y. Ono, and T. Kajitani, Jpn. J. Appl. Phys., Part 2 **41**, L849 (2002).
[18] J. Sugiyama, C. Xia, and T. Tani, Phys. Rev. B **67**, 104410 (2003).
[19] J. Sugiyama, J. H. Brewer, E. J. Ansaldo, H. Itahara, K. Dohmae, Y. Seno, C. Xia, and T. Tani, Phys. Rev. B **68**, 134423 (2003).
[20] J. Sugiyama, J. H. Brewer, E. J. Ansaldo, H. Itahara, K. Dohmae, C. Xia, Y. Seno, B. Hitti, and T. Tani, J. Phys.: Condens. Matter **15**, 8619 (2003).
[21] T. Takami, Y. Umeshima, H. Nanba, and M. Itoh, J. Phys.: Conf. Ser. **150**, 042199 (2009).
[22] W. Koshibae, K. Tsutsui, and S. Maekawa, Phys. Rev. B **62**, 6869 (2000).
[23] M. Karppinen, H. Fjellvåg, T. Konno, Y. Morita, T. Motohashi, and H. Yamauchi, Chem. Mater. **16**, 2790 (2004).
[24] T. Tani, J. Korean Phys. Soc. **32**, S1217 (1998).
[25] T. Tani, H. Itahara, C. Xia, and J. Sugiyama, J. Mater. Chem. **13**, 1865 (2003).
[26] Y. Miyazaki, M. Onoda, T. Oku, M. Kikuchi, Y. Ishii, Y. Ono, Y. Morii, and T. Kajitani, J. Phys. Soc. Jpn. **71**, 491 (2002).
[27] H. Nakatsugawa, H. M. Jeong, R. H. Kim, and N. Gomi, J. Phys. Soc. Jpn. **46**, 3004 (2007).
[28] C. D. Ling, K. Aivazian, S. Schmid, and P. Jensen, J. Solid State Chem. **180**, 1446 (2007).
[29] R. Ray, A. Ghoshray, K. Ghoshray, and S. Nakamura, Phys. Rev. B **59**, 9454 (1999).
[30] M. Sano, S. Horii, I. Matsubara, R. Funahashi, M. Shikano, J. Shimoyama, and K. Kishio, Jpn. J. Appl. Phys., Part 2 **42**, L198 (2003).
[31] Y. Wakisaka, S. Hirata, T. Mizokawa, Y. Suzuki, Y. Miyazaki, and T. Kajitani, Phys. Rev. B **78**, 235107 (2008).
[32] M. Kontani, T. Hioki, and Y. Masuda, J. Phys. Soc. Jpn. **39**, 672 (1975).
[33] S. Arita and T. Takeuchi (private communication).
[34] H. R. Krishnamurthy, C. Jayaprakash, S. Sarker, and W. Wenzel, Phys. Rev. Lett. **64**, 950 (1990).
[35] M. Fujita, M. Ichimura, and K. Nakao, J. Phys. Soc. Jpn. **60**, 2831 (1991).
[36] B. Davoudi, S. R. Hassan, and A.-M. S. Tremblay, Phys. Rev. B **77**, 214408 (2008).
[37] P. Limelette, V. Hardy, P. Auban-Senzier, D. Jérome, D. Flahaut, S. Hébert, R. Frésard, Ch. Simon, J. Noudem, and A. Maignan, Phys. Rev. B **71**, 233108 (2005).
[38] Y. Ando, N. Miyamoto, K. Segawa, T. Kawata, and I. Terasaki, Phys. Rev. B **60**, 10580 (1999).
[39] T. A. Tyson, Z. Chen, Q. Jie, Q. Li, and J. J. Tu, Phys. Rev. B **79**, 024109 (2009).
[40] G. Mahan, B. Sales, and J. Sharp, Phys. Today **50** (3), 42 (1997).